Silicon-based electrodes formulation in buffered solution for enhanced electrode-electrolyte interfaces

Aude Roland, Benoit Delarre, Jean-Bernard Ledeuil, Nicolas Louvain, Hervé Martinez, Laure Monconduit

▶ **To cite this version:**

Aude Roland, Benoit Delarre, Jean-Bernard Ledeuil, Nicolas Louvain, Hervé Martinez, et al.. Silicon-based electrodes formulation in buffered solution for enhanced electrode-electrolyte interfaces. Journal of Power Sources, 2021, 489, pp.229465. 10.1016/j.jpowsour.2021.229465 . hal-03153640

HAL Id: hal-03153640
https://hal.science/hal-03153640

Submitted on 26 Feb 2021

HAL is a multi-disciplinary open access archive for the deposit and dissemination of scientific research documents, whether they are published or not. The documents may come from teaching and research institutions in France or abroad, or from public or private research centers.

L'archive ouverte pluridisciplinaire **HAL**, est destinée au dépôt et à la diffusion de documents scientifiques de niveau recherche, publiés ou non, émanant des établissements d'enseignement et de recherche français ou étrangers, des laboratoires publics ou privés.

Silicon-based electrodes formulation in buffered solution for enhanced electrode-electrolyte interfaces

Aude Roland[a], Benoit Delarre[a], Jean-Bernard Ledeuil[b], Nicolas Louvain[a,c], Hervé Martinez[b,c], Laure Monconduit[a,c]

a. Institut Charles Gerhardt Montpellier, Université de Montpellier, CNRS, ENSCM, Montpellier, France

b. CNRS/ UNIV Pau & Pays Adour/ E2S UPPA, Institut des Sciences Analytiques et de Physicochimie pour l'Environnement et les Matériaux, UMR5254, 64000, Pau, France

c. Réseau sur le Stockage Electrochimique de l'Energie (RS2E), FR CNRS 3459, 33 Rue Saint Leu, 80039 Amiens, France

E-mail: Laure.monconduit@umontpellier.fr

Abstract

Silicon nanoparticles based composite electrodes for Li-ion batteries reach high specific capacities and enhance cyclability compared with larger silicon particles. Such electrodes are foreseen for the next generation Li-ion batteries (LiB). Playing on binder and conductive additives in the formulation of the Si based electrodes is a well-known strategy to to enhance performance. Aqueous electrode formulations using the carboxymethyl cellulose as environmentally friendly binder has already showed great cyclability enhancements, especially when employed in acidic conditions. In this study, pH = 1, 3 and 7 buffered solutions were studied as solvent to prepare the Si/C/CMC composite electrodes.

The influence of the formulation pH on the electrode components interactions were followed through a combined ATR-FTIR / XPS experiment and discussed in relation with the electrode electrochemical performance. Interestingly, the pH=7 buffered solution show increased capacity retention and coulombic efficiency during 100 cycles compared with the electrode obtained in acidic conditions. Post mortem analysis and EIS study highlighted differences of electrode/current collector (CC) adhesion and SEI deposition.

Keywords :

Battery, Li-ion, Silicon, nanoparticle, formulation, pH

1. Introduction

Thanks to its high capacity and its low working potential, silicon is a great candidate as negative electrode for the next generation of Li-ion batteries. [1,2] However, silicon lithiation/delithiation induces large volumetric variations which lead to particle break and electrode delamination. Consequently, silicon exhibits poor cycling performance which limits its integration into commercial devices.[3] Nanostructuration lowers mechanical stress and hence limits Si particles pulverization but also increases ionic conductivity and Si reactivity vs Li. [2,4,5] The formulation of composite electrodes with conductive carbon additives compensates the low electronic conductivity of silicon and enhances electrochemical performance. [6,7]. The binder plays a key role on electrodes mechanical properties, and as far as we know, for silicon-based negative electrodes the best performance were obtained with aqueous binders such as carboxymethyl cellulose (CMC) or polyacrylic acid (PAA) even if CMC presents a lower mechanical strength than PVdF or CMC/SBR mix. This unexpected result introduced new considerations for chemical interactions between electrode components.[8] Lestriez *et al.* studied the influence of the formulation pH on electrochemical performance and showed higher cyclability for silicon based electrodes prepared with a controlled pH around 3. This result was explained by the formation of an extensive polymer network through inter-component interactions, enhancing Si and carbon additives dispersion in the electrode. [9] Covalent bond were demonstrated between CMC carboxylic acid groups and Si native oxide at pH=3, demonstrating the critical role of this silicon native oxide [10] as well as the positive impact of substitution COOH groups by COONa.[11–13] Moreover longer CMC chains appear to better connect the particles [6] and contrarily smaller counter ions (Li^+ vs Na^+, K^+) isolate them by limiting the COO-Si interactions. Finally, it was shown that the absence of interaction as well as too strong (covalent) interaction limit the electrode cycling performance. Weaker bond, as hydrogen, could help to maintain a good stability by bringing self-healing properties. [6] The electrochemical behavior of the electrodes presenting covalent Si-CMC interactions showed enhanced cycling performance when the capacity is limited, while electrodes with hydrogen Si-CMC interactions performed better on the overall range potential. [14]

The three possible binder/silicon interactions can be summarized [15] by:

- The physical “sticking function” that connects silicon grains between each other and with the copper foil, as observed with PVdF. This binder glue is not able to compensate extreme tension and results in a partial silicon particles isolation while cycling.
- With CMC or PAA containing carboxylic acid groups, silicon interacts in two different ways, i) by covalent bond (observed in acidic formulation condition pH=3), in this case the volumetric

expansion is partially buffered, but the strong bonds can break or cause a break of the particles or ii) by hydrogen bonds, in this case, bonds can form and deform in order to reorganize the electrode in its more stable configuration limiting electrode delamination and particles pulverization. They also showed a stronger carbon-CMC film adhesion with a silicon wafer surface at neutral pH, which indicates that silicon/CMC interaction could be maximized by limiting CMC interchain interactions.
Also, enhanced coulombic efficiency and cyclability was observed by modulating the ratio hydrogen/covalent bond between silicon particles and binder, through a post treatment called maturation (80 % of humidity), the electrode showed an optimum between stiffness and flexibility maintaining electronic contacts and buffering the volumetric changes. [16] Finally, the pH=3 formulation showed an impact on the reorganization of the polymer at the contacts points between silicon particles and CC limiting electrode delamination, and promoting the formation of a thinner and less resistive SEI. [17,18]

To sum-up, the acidic condition (pH=3) induces the ester bond formation between silanols (silicon particles surface groups) and carboxylic acid groups from the CMC binder enhancing Si dispersion within the electrode but also adhesion to the CC whereas a neutral pH limits CMC-CMC interaction increasing the Si-CMC weak interactions.
The present study focus on the pH effect on the interactions between the Si based composite electrode components (Si, binder, CC) and its effect on battery performance. pH = 1, 3 and 7 buffered solutions and CMC were used as solvent and binder respectively to prepare Si nano based composite electrodes and compared with an electrode formulated with distilled water. In order to explain the enhanced capacity retention and coulombic efficiency observed for pH7, the inter-component interactions (Si-CMC, CMC-CMC, and electrode-CC) were investigated by ATR-FTIR and XPS while the electrochemical behavior were compared by galvanostatic cycling and impedance spectroscopy analysis. Post mortem SEM and XPS analysis on the electrodes were realized to visualize and compare the film/CC adhesion and the SEI formation.

2. Experimental part

2.1. Silicon-binder interaction characterization:

ATR-FTIR and XPS measurements were performed on Si-CMC films obtained with the buffered solution (pH = 1, 3, or 7, named pH1, pH3 and pH7) (SI 1) as solvent and without carbon to limit the absorption signal.[19] The Si/C proportions were calculated to be close to those used in the electrochemical tests. Films were deposited on Mylar foil, dried one night at room temperature and then 2 hours under vacuum (Buchi) at 80 °C. FTIR-ATR were performed using a spectrum two (Perkin Elmer) (32 scans - resolution 4).

XPS measurements were performed on a Thermo Scientific K-alpha spectrometer equipped with a 120 mm mean radius Hemi-spherical Analyzer (HSA) and a micro-focused monochromated radiation (Al Ka,1486.6 eV, micro-spot continuously variable from 30 to 400 µm diameter) operating under UHV conditions (residual pressure of 1.10^{-7} Pa). The HSA to surface angle is 90° (TOA angle) so the photoelectrons are collected from the maximum depth and according to the high Kinetic Energy (about 1400 eV) the sampling depth is about 6 nm. The X-ray power is operating at 72 W (12 kV, 6 mA) for a typical 400 µm beam diameter. The spectrometer is fitted with a dry argon glove box directly connected to the fast entry load lock to prevent sample exposure to air and moisture (concentration of H_2O and O_2< 1ppm).
The spectra are recorded in the constant Pass Energy (PE) mode CAE (Constant Analyser Energy), both for wide high sensitivity survey spectra (PE=200 eV) and high energy resolution analyses (PE=20 eV) for chemical quantitative resolved analyses. Charge effects are compensated by the use of a dual beam charge neutralization system (low energy electrons and Ar^+ ions flood), which has the unique ability to provide consistent charge compensation. All the neutralizer parameters remain constant during the analysis and allow one to calibrate C 1s binding energy for adventitious carbon at 285.0 eV. Spectra are mathematically fitted with Casa XPS software using a least squares algorithm and a non-linear baseline (Shirley). The fitting peaks of the experimental curves are defined by a combination of Gaussian (70%) and Lorentzian (30%) distributions. The quantification is performed using Thermo Scientific relative sensitivity factors based on the Scofield Cross-sections. The species proportions have been calculated from atomic percentages extracted from quantifications tables. XPS spectra and quantification tables of PH3, PH5, PH7 samples (pristine, OCV, first and fiftieth electrochemical cycle) are displayed in SI 2.
SEM images were recorded with a Hitachi S-4800, isolating sample may have been C or Pt coated. EDX mapping were performed using a Zeiss Evo HD15 equipped with SDD EDX oxford Instruments X-MaxN detector (50 mm² SDD), the operating conditions were 10kV accelerating voltage, 8 - 9 mm working distance, and 300000 counts.
Zeta potential were measured with a Zeta sizer 3000 (Malvern) using a folded capillary Zeta Cell (DTS1070).

2.2. Electrochemical performance evaluation:

Silicon nanoparticles (diameter 80 nm (SI 3)) obtained by laser pyrolysis were used as active material. Super P (H30253 Carbon black Alpha Aesar) and Vapor growth fibers (VGCF-H, BET = 15 $m^2 g^{-1}$, Showa Denko) were used as conducting agent in a 50:50 wt ratio and sodium

carboxymethyl cellulose (MW = 250 000; DS = 0.9, Sigma Aldrich) as binder. The Si:VGCG/SP:CMC weight ratio was 18:70:12. The first step consisted in mixing the active material and the carbon additives in an agate mortar and in a planetary mill for 10 min (500 rpm / 3 balls) to increase the electronic percolation in the electrode. [20] The second step consisted in adding the binder and the solvent (around 1 mL +/- 0.3 mL : distilled water or buffered solution pH = 1, 3 or 7) (SI 1) and homogenize for 1 hour with ball-milling (500 rpm / 3 balls). Then the slurry was spread on copper foil with a controlled thickness of 150 nm using a 3540 bird film applicator from Elcometer, and subsequently air-dried at room temperature for 24 h. The electrodes were punched into 12.7 mm-diameter disks and dried at 80 °C under dynamic vacuum overnight. The dry electrodes were not calendared. The total material loading was approximately 1.2 mg cm^{-2} (0.25 mg/cm^2 for Si), corresponding to a density of 0.4 g cm^{-3} approximately. Coin cells (2032) were assembled in an Argon filled glovebox, the electrochemical cycling performance was carried out in half cell (vs lithium), the two electrodes were separated by a glass-fiber paper (GF/D, Whatman) soaked with the electrolyte ($LiPF_6$ 1M in EC/PC/3DMC (Solvionic) + 5%v of FEC (98% purity, Alfa Aesar) and 1%v VC (80 ppm BHT as stabilizer, 99% purity)).

The electrochemical galvanostatic measurements were performed between 1.5 and 0.01 V vs Li^+/Li at a current density of C/20 (178 mA g^{-1}) for the first cycle, and then at C/5 (716 mA g^{-1}) for the further cycles. The weight of carbons (Super P, carbon fibers) and the silicon particles were considered for the gravimetric capacity calculation (per gram of silicon and carbon). The expected specific capacity is approximately 775mAh g^{-1}(Si/C). This capacity is calculated by considering the molar composition of the composite from its mass composition ($C_{0,9}Si_{0,1}$), and the values of the experimental capacity of the carbon composite (185 mAh g^{-1}) and theoretical capacity of silicon (3580 mAh g^{-1}) considering the formation of the alloy $Li_{15}Si_4$ as an end-product of the lithiation. The calculation of the expected capacity is detailed in SI 4. In all case, it is important to note that capacity value is not perfectly reproducible, these variations come from the masse evaluation depending on the electrode homogeneity. The following tests were carried out using a Biologic BCS-805 battery cycler at 25 °C. All the electrochemical measurements were repeated a minimum of three times.

Variable current density tests have also been carried out from C/20 to 20C to investigate the rate capability.

3. Results and discussion

3.1. Si-CMC interactions in pH1, pH3, pH7 and pH5 electrodes.

The visual observation of the films obtained by using buffered solutions showed important texture differences (SI 5) which can be interpreted as various interactions between components in the electrode. The electrodes formulated in pH 1 and 3 acid conditions appear as self-standing films, likely with stronger polymer interchain interactions than in the electrodes obtained with distilled water or with pH7 buffered which look like powders once peeled-off from Mylar support.

FTIR-ATR spectra for CMC based films (Figure 1-a) and for CMC-Si based films (Figure 1b) exhibit all one broad and intense band at 3300 cm^{-1} typical from –OH groups, slightly shifted to lower wavenumber than expected for primary hydroxyl group (3670 cm^{-1}), most probably indicating interchain hydrogen bonds.[21] Other bands are observed at 2900 cm^{-1} (–CH bond stretching), at 1590 cm^{-1} ($–COO^-$ groups), two sharp bands at 1410 et 1323 cm^{-1} ($-CH_2$ scissoring and –OH stretching vibration), at 1269 and 1204 cm^{-1} (likely due to the presence of a CH second overtone or a combination or stretching vibrations of the C-O-C group.), at 1030 cm^{-1} (C-O-C stretching), a shoulder at 1100 cm^{-1} (ether groups $-CH-O-CH_2-$), and at 911 cm^{-1} (–OH groups rotation).[21] For pH1 and pH3, spectra show a new band at 1730 cm^{-1} corresponding to the –COOH groups coming from COO^- group protonation. The band observed at 1240 cm^{-1} could be due to CMC hydrogen bond formation. [21]

By adding the Si particles, the ester bond Si-OOC(CMC) expected at 1630 cm^{-1} appears for pH1, however less visible at pH3. [13] A relative slight intensity decrease is observed for the carboxylic acid and OH bands compared with the C-O bond for pH7 samples (Figure 1b). At 3300 cm^{-1}, the -OH band intensity drop was expected with an increasing pH (> 3, 5)[7], indeed in this case the Si surface should be covered with O^-. Experimental zeta potential measurements were realized and showed a globally non-charged surface in all the buffered solutions (SI 6) with the zeta potential value lower than 25mV which is too low to be considered as a charged surface. This indicates that the Si surface still exhibits silanols groups.

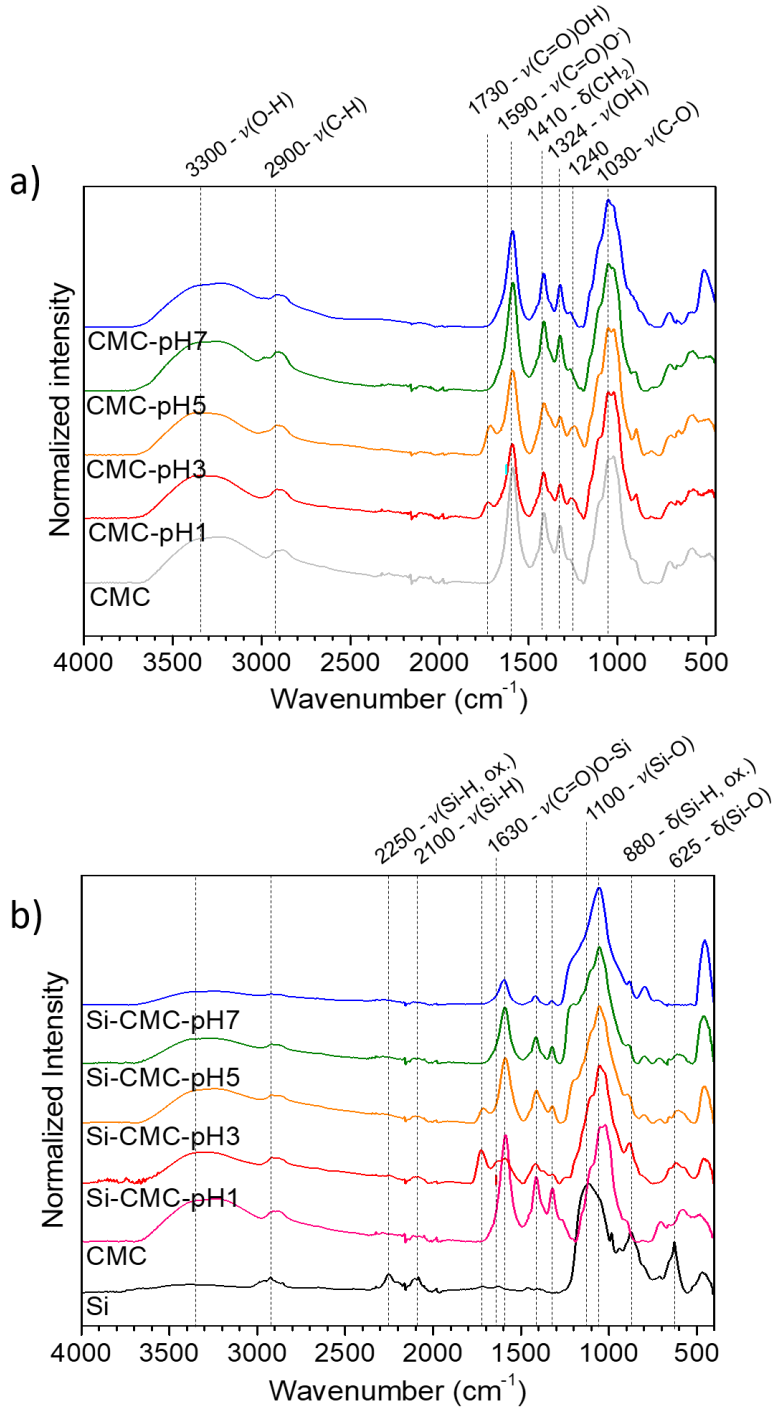

Figure 1 : ATR-FTIR curves for a) CMC electrodes and b) CMC + Si electrodes.

Complementary XPS measurements were carried out, on the Si-CMC films (Figure 2).

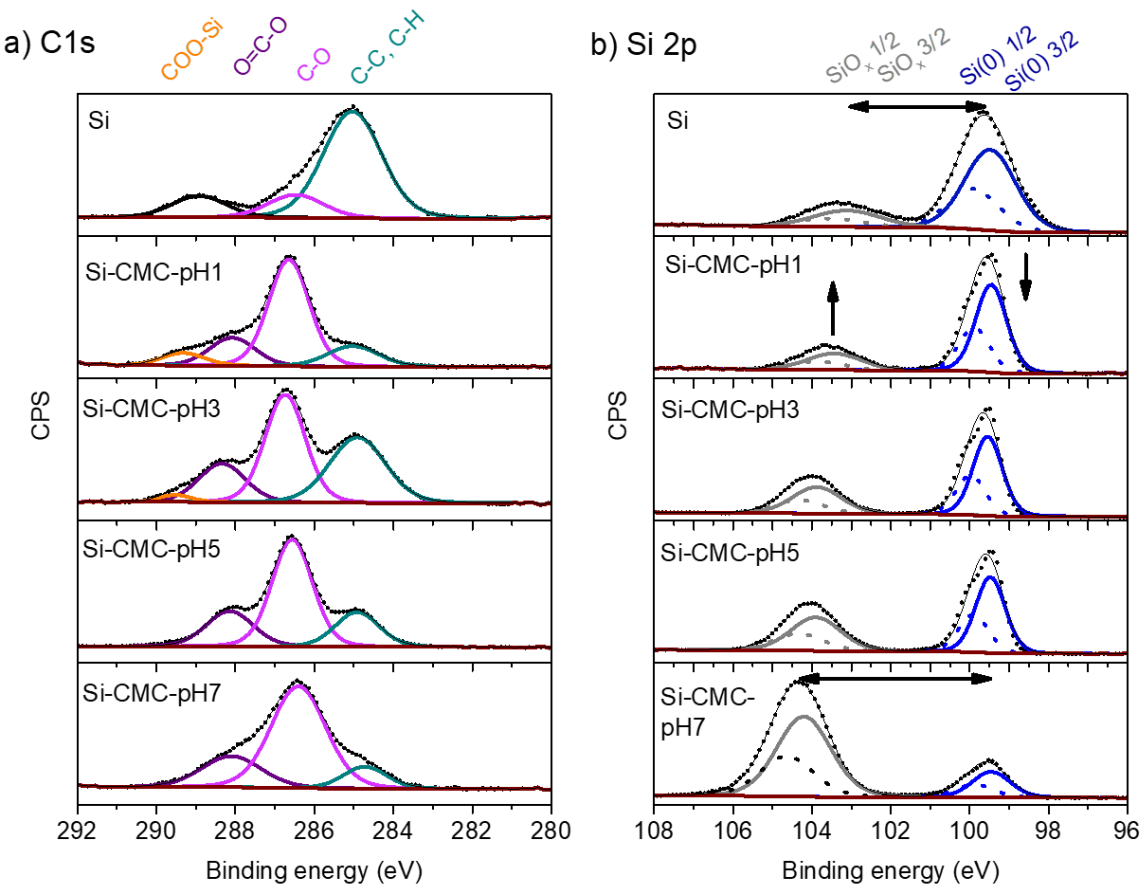

Figure 2 : XPS of a) C 1s, b) Si 2p spectra for Si-CMC films as a function of pH of the electrode formulation.

C 1s spectra (292-280 eV) shows 3 to 4 contributions; at 285 eV corresponding to C-C and C-H bonds, at 286.5 eV corresponding to C-O bonds, at 288.5 eV corresponding to COO. For pH1 and pH3, one other pic appears at higher binding energy which could be attributed to the ester bond COO-Si. [22] Si 2p spectra exhibits 4 contributions, 2 components between 99 and 101 eV attributed to Si (0) (2p3/2 and 2p1/2) and two components at higher binding energy (102-106 eV) attributed to silicon oxide (2p3/2 and 2p1/2 of SiO_x with x<2). For highest pH, an increase in the intensity as well as a shift toward higher binding energy are observed for the peak attributed to silicon oxide, indicating higher surface oxidation while increasing the formulation pH. The corresponding binding energy of pH7 is characteristic of SiO_2.

3.2. Component distribution in the electrode:

EDX mapping were recorded for all the series of Si electrodes prepared at different pH. The top and cross-section views (Figure 3) show the elements (Cu, O, Na, Si, C) dispersion across the electrodes.

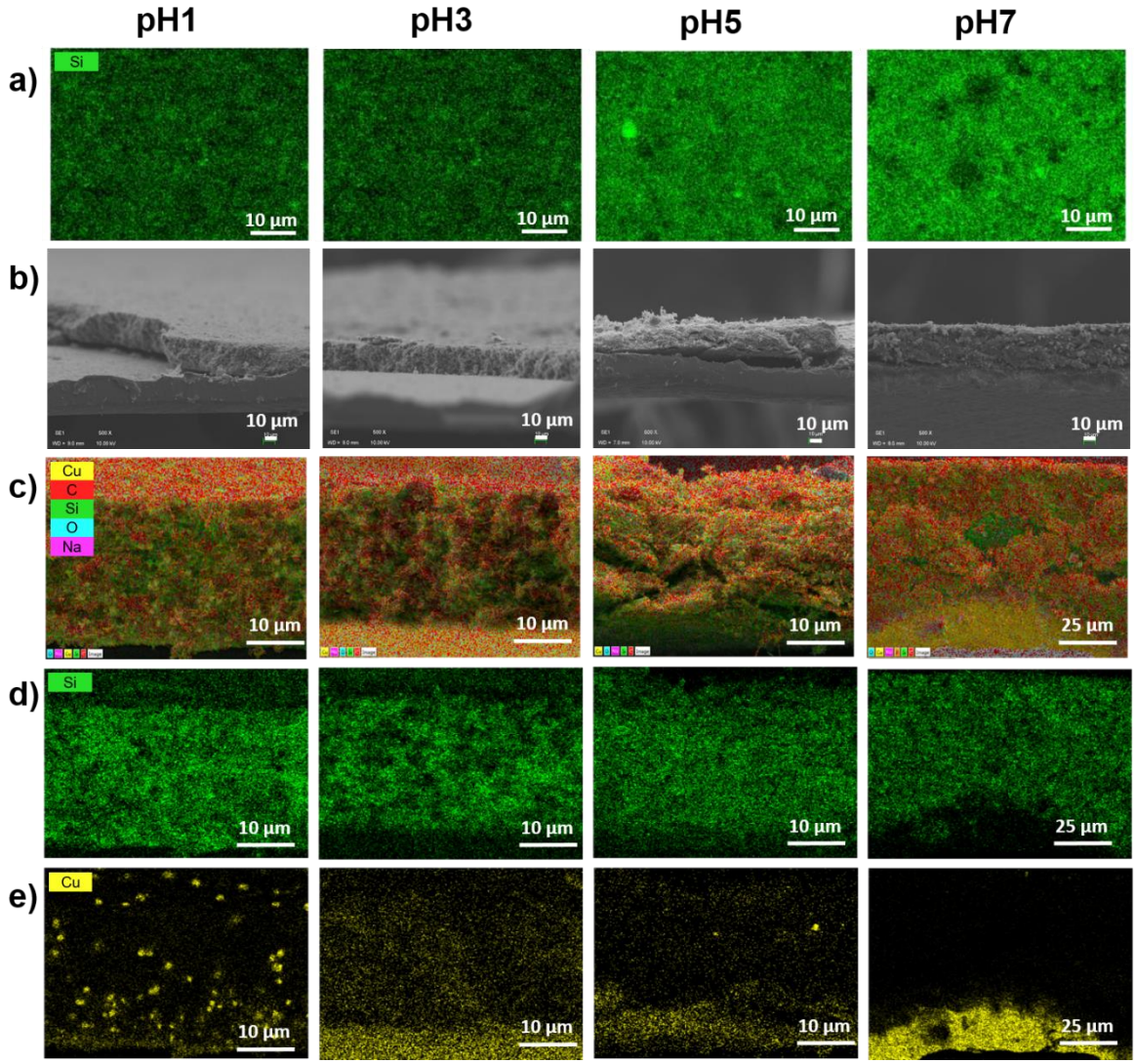

Figure 3 : a) Si Kα1 EDX mapping of the surface, b) cross-section SEM image, c) EDX superposition of all elements Si, Cu, Na, C for the cross-section, d) Si Kα1 EDX and e) Cu Lα1-2 EDX of the electrodes prepared at the different pH.

Electrodes formulated in acidic conditions (pH1 and pH3) seem darker which probably comes from the polymer grafting at the silicon particles surface screening the Si signal. The cross-section views for pH1 and pH3 show a copper contribution across the electrode thickness, confirming the already observed Cu dissolution from the current collector (CC) in acidic conditions and its migration through the electrode. [18] In neutral condition (pH5), the copper presence is much lower and likely only due to contamination coming from cutting. From literature review, the presence of Cu^{2+} could induce coordination bonds within the polymer network enhancing cycling stability.[18] For pH7, the Cu presence is limited and only observed at the CC proximity. Moreover, no delamination from the CC is observed for pH7, indicating a good electrode/CC adhesion.

3.3. *Formulation pH influence on electrochemical performance*

Battery performance, as the coulombic efficiency (CE) and the capacity as function of cycle number were measured from galvanostatic curves (: a) 1st cycle galvanostatic curves and b) cyclability over 100 cycles (with a current 0.4 A $g^{-1}_{(Si+C)}$ for the 1st cycle and 1.5 A $g^{-1}_{(Si+C)}$ for next cycles) as a function of the pH of the electrode formulation.

). Note that galvanostatic curves (Figure 4 a) were normalized to compare easily the first cycle shape and compare the irreversibility.

During the first discharge (Figure 4 a), a rapid potential drop is observed until 0.1V, this drop is quicker for the electrode pH7 (and then for pH5 > pH3 a pH1) indicating a lower SEI formation, which is correlated with a best mean CE for the first cycle (CE1), pH1: 64 %, pH3: 70 %, pH5: 74 % and pH7: 75 % (*Table 1*). The cyclability of the electrode formulated at pH7 is also enhanced with a mean capacity retention after 100 cycles around 87 % of the initial reversible capacity, compared to 77% for pH1, 81 % at pH3 and 67 % for pH5 (*Table 1*). Even though the capacity of first cycles is lower for higher pH, the mean value over three batteries confirm the enhanced performance for pH7.

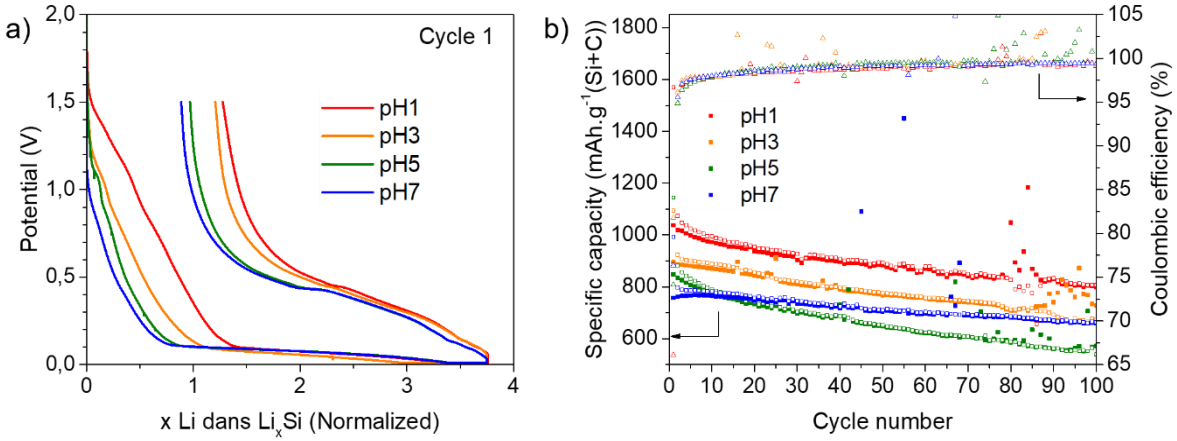

Figure 4: a) 1st cycle galvanostatic curves and b) cyclability over 100 cycles (with a current 0.4 A $g^{-1}_{(Si+C)}$ for the 1st cycle and 1.5 A $g^{-1}_{(Si+C)}$ for next cycles) as a function of the pH of the electrode formulation.

	D1	StdDev. (SI 7)	CE1%	C1	C50	C100	C100/C1	CE100%
pH1	1538	131	64	1037	883	799	0.77	99.1
pH3	1291	108	70	895	768	728	0.81	99.6
pH5	1158	95	74	848	649	571	0.67	99.5
pH7	1061	86	75	757	705	659	0.87	99.4

Table 1 : Performance of the different electrodes as function of the pH. Mean values from 3 galvanostatic measurements

The evolution of the electrodes impedance while cycling was followed by electrochemical impedance spectroscopy (EIS). EIS measurements were realized in three electrodes set-up [23] with Li at the working and counter electrodes in order to remove the counter electrode impedance contribution. Impedance spectra were recorded at different state of charge, after 24 hours of open circuit voltage (OCV), at the end of first discharge and at the end of 10^{th} discharge. The results were normalized by the Si loading in the electrode to obtain consistent trends. The Nyquist plot of EIS data (Figure 5) shows a semi-circle attributed to faradaic and capacitif phenomenons at interfaces followed by a linear curve attributed to ions diffusion within the electrode. The semicircle originates from the sum of the charge transfer resistances related to interfaces through which electrons pass, such as electrolyte / active material or active material / CC interfaces. In a composite electrode, this interfaces are difficult to differenciate and only a global charge transfer resistance, meaning taking in consideration the sum of charge transfer resistances, will be discussed. A larger diameter indicates a higher charge transfer resistance.

After 24h OCV (Figure 5), the largest charge transfer resistance is observed for pH5 electrode followed by pH3, pH1 while the lowest is for pH7. The lowest charge transfer resistance for pH7 electrode could be due to strong adhesion properties to the CC enhancing the electronic percolation (Figure 3). The higher resistance for acidic formulations are probably due to the polymeric wrap of the Si particles coming from the Si-CMC covalent interactions and limiting electronic/ionic conduction.[10,13]

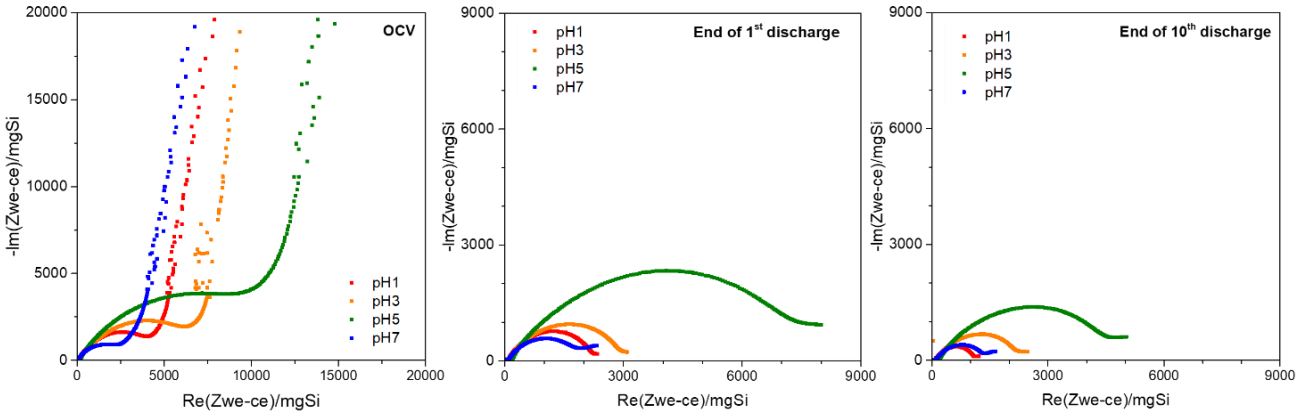

Figure 5 : Nyquist representation of electrochemical impedance spectroscopy for Si based electrodes formulated at pH=1, 3, 5 and 7.

After the first discharge, the charge transfer resistances reduce, likely due to i) a better electronic percolation coming from the volumetric expansion which leads to a better contact between the electrode components as well as to ii) a higher ionic conductivity of the lithiated phases. It is worth noticing that the low CE1 observed at the first cycle for the whole series is more attributable to a chemical SEI formed during the OCV than to an electrochemical one formed during the first discharge, as the charge transfer resistance decreases.

After 10 cycles, the lower impedance observed for all samples could be attributed to the improvement of the ionic path. It demonstrates that the SEI layer is non-blocking at this step. The lowest resistance of the pH7 is in good agreement with the limited SEI formation observed from the first discharge of galvanostatic curves in comparison with the electrodes prepared at lower pH.

Erreur ! Source du renvoi introuvable. shows the cumulative relative irreversible capacities (RIC) associated with the SEI formation and the electronic disconnection. The RIC calculation is based on the studies published by Gauthier et al. and is defined as the ratio between the irreversible loss capacity and the delivered charge capacity.[24,25] This capacity loss can be divided into two contributions, one coming from the SEI formation and the second from the particle disconnections. In this case, it is assumed that the irreversibility due to disconnections is mostly created during the charge, when the particles deflate upon dealloying, while the irreversibility due to the SEI formation is almost exclusively generated during the discharge.

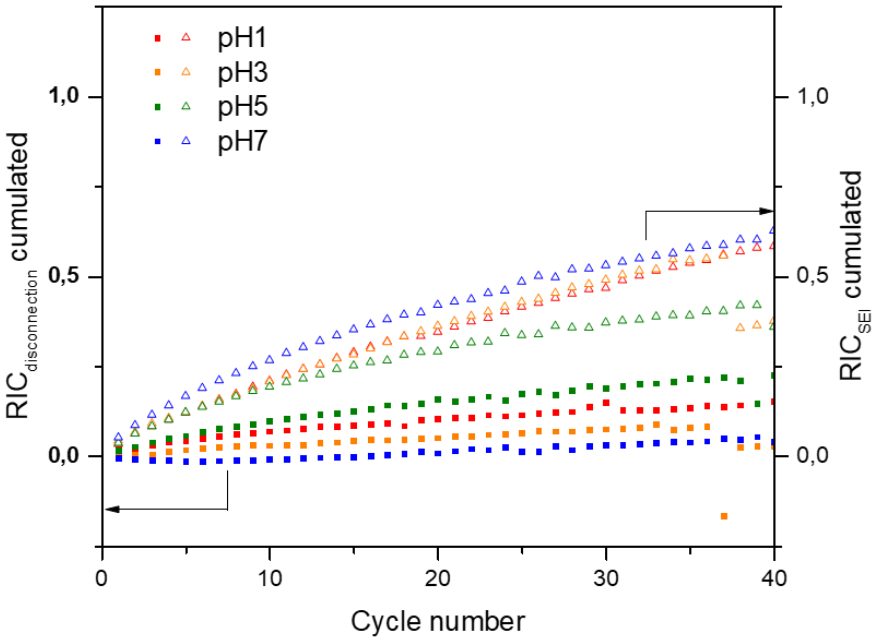

Figure 6 : Cumulated RIC for pH1, pH3, pH5 (distilled water) and pH7 Si-based electrodes

For all samples, the higher values of RIC_{SEI} seem to indicate a capacity loss mainly coming from SEI formation. However, the highest $RIC_{disconnection}$ observed for pH5 could indicate a weak adhesion to the CC both explaining the highest charge transfer resistance (Figure 5) and its lowest RIC_{SEI} as a direct consequence of disconnections by limiting the electrode active surface area. This behavior would be responsible for its poor capacity retention. In comparison, pH7 shows enhanced CC adhesion (low $RIC_{disconnection}$) in good correlation with the lowest charge transfer resistance (Figure 5) and probably responsible for the higher RIC_{SEI}. Moreover, RIC_{SEI} from pH7 stabilizes as a function of the cycle number compared with pH1 and pH3 which increase continuously. This stabilization for pH7 likely indicates a limited electrolyte degradation and the formation of a more efficient SEI.

Finally, RIC representation failed to fully explain the best performance for pH7. To go further, the following parts focus on the chemical characterization of the SEI and the impact of the pH on CC.

3.4. pH formulation influence on the SEI formation

The pH1, pH3, pH5 and pH7 electrodes were characterized after 50 cycles in charge. **Erreur ! Source du renvoi introuvable.** shows the SEM images for electrodes before and after cycling. Before cycling, pH1 electrode exhibits a homogeneous surface, with a high visible porosity while pH3 electrode shows a heterogeneous surface with lighter stripes attributed to the binder.

pH7 electrode is homogenous and the porosity seems lower. At pH5 homogeneous surface is observed with an intermediary porosity between pH7 and pH3.

After cycling, pH3 and pH7 appeared cracked indicating mechanical weaknesses within the electrode (probably coming from stronger CMC-CMC interactions) and privileged interaction with the CC. [26] This hypothesis is in good agreement with RIC calculations showing a limited disconnection at pH7. However, some differences are observed in the SEI deposition at the electrode surface: pH3 and pH5 electrode porosity seem completely blocked after 50 cycles whereas it is only partially blocked for the pH1 electrode. For pH7 electrode, it is still possible to distinguish carbon additives, indicating a very thin SEI layer. This fits with the electrochemical results (best initial CE and best capacity retention over 100 cycles) and also with the lowest electrode impedance observed in cycling.

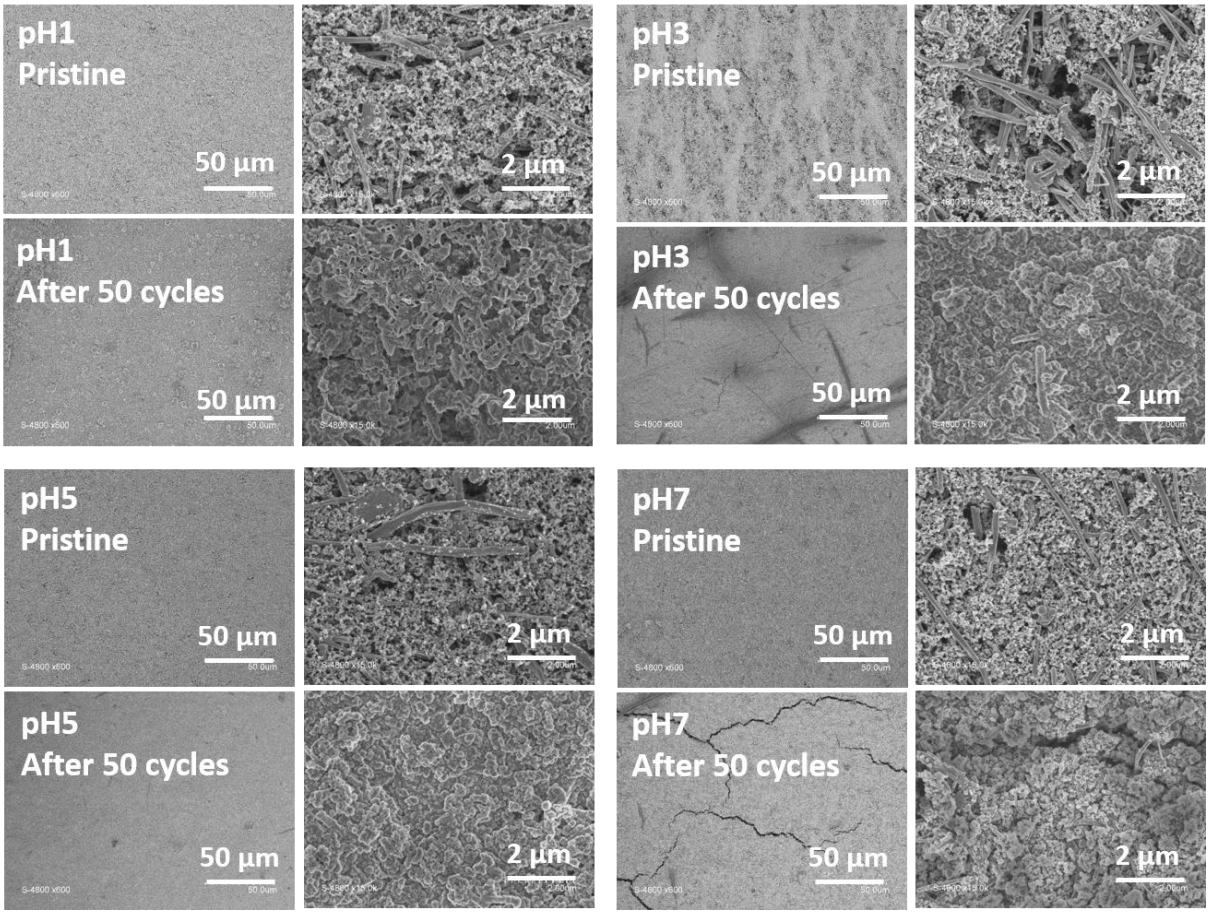

Figure 7 : SEM image for pH1, pH3, pH5 and pH7 electrodes before and after 50 cycles (end of charge after 3 rinsing with DMC).

To identify the SEI species, XPS spectra have been recorded at different state of charge and discharge (1^{st} and 50^{th} cycles). For pristine electrodes, XPS measurements show very close compositions (SI 8). After contact with the electrolyte, LiF, Li_2CO_3 and Li_2O species were clearly identified on the electrode surface. The amount of phosphate and/or fluoro phosphates

detected was very low and thus considered as negligible. Figure 8 summarizes the SEI components evolution as a function on the state of charge for the different electrode formulations. After OCV, all the electrodes showed close surface compositions with a major LiF proportion and a low Li_2CO_3 one. At the end of the 1st discharge, Li_2CO_3 proportion increases and represents the major contribution for pH7. Li_2O is identified at all the electrode surfaces. At the end of the first charge, an important Li_2CO_3 dissolution is observed for pH3 and pH7 electrodes, this dissolution seems more limited for the pH5 electrode. At the 50th cycle, Li_2CO_3 formation-dissolution phenomenon is still detected on all electrodes surfaces, and particularly pronounced for the pH7 electrode. At the 50th charge, a strong Li_2O accumulation is observed for the electrodes pH5 and pH3.

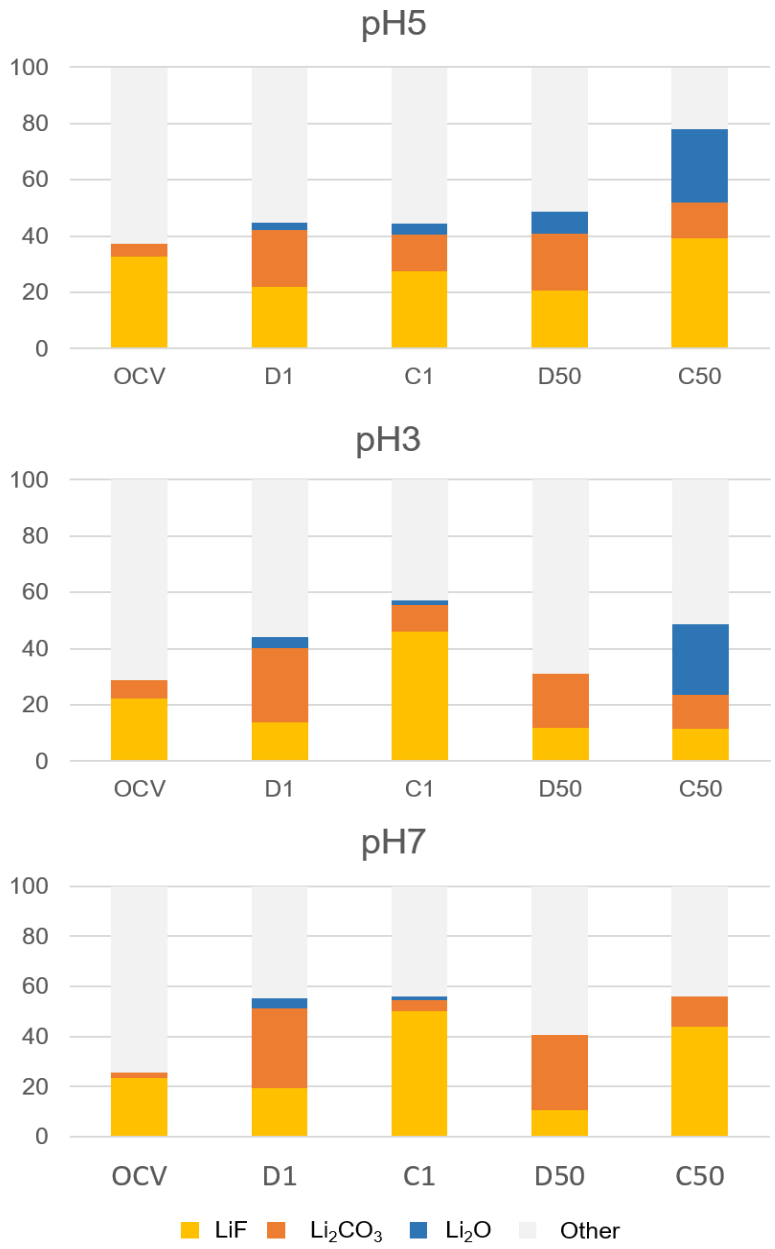

Figure 8 : Evolution of the SEI composition with cycles as function of the electrode preparation pH.

LiF and Li_2CO_3 proportions seem less stable between charge and discharge for buffered formulations. Li_2O proportion is higher and accumulates with cycles for pH3 and pH5, while it is very low for electrode pH7. Li_2O is poorly soluble in the electrolyte [27], and can limit lithium diffusion at the electrode surface, which can explain the lowest impedance of the cycled pH7 electrode (see EIS part). The SEI formation/dissolution is slightly exacerbated at pH=7. At that point, it seems that a very stable SEI is not needed for enhanced performance, a less stable SEI could limit the pore obstruction (as observed by SEM images) and have a positive influence in cycling.

3.5. pH formulation influence on the current collector

Limited RIC_{SEI} was observed for pH7 electrode compared with other buffered solutions, this was partially explained by the SEI nature and its evolution in cycling. SEM and XPS analyses have also shown Cu traces on top and through the electrode thickness, especially at lowest pH. Complementary SEM and XRD characterization of the CC were realized after being exposed 24 hours to the different buffered solutions. The SEM images (SI 10) showed the formation of different layers at the CC surface. For pH1, the surface is covered by a dark layer, and the solution turns blue showing the Cu^{2+} presence; for pH3 the CC is less corroded and the solution turns slightly blue; for pH5 (with distilled water), the CC surface is unaffected; finally for pH7, the solution is very slightly colored and the surface is slightly attacked. After room temperature drying, a blue layer is formed at the surface of the CC in contact with pH1 and pH7 solution; for pH3 the CC shows rust like spot, and for pH5 the surface appears as new. SEM (Figure 9) and EDX analysis in SI 9 show for pH1 the formation of a micro-ball structures forming a blue layer composed by Cu, O and Cl elements. This layer does not attach strongly to the surface and peel off easily. For pH3, the surface displays ribs composed by Cu, O and Cl. For pH5, the surface is smooth and EDX indicates a major composition of Cu with a slight contribution from O probably corresponding to a low surface oxidation. Finally, for pH7, excepting the presence of crystals coming from the salt from the buffered solution, the surface appears after drying only slightly modified by a blue layer. This soaking test proves the strong impact of the pH electrode formulation also on the CC. The pH=7 buffered solution leads to the formation of a copper oxide layer which enhances likely the electrode adhesion (Figure SI5).

XRD measurements (**Erreur ! Source du renvoi introuvable.** 11) were realized to characterize the nature of the crystalline phases formed at the CC surface in contact with the different pH solutions. For pH1, CuCl, $CuCl(OH)_3$ and Cu (0) are identified. For pH3, CuCl and Cu (0) is observed (Cl is coming from the acid used to decrease the pH). For pH5, only Cu(0) is observed. For pH7 Cu_2O, Cu(0) and the salt from the buffered solution are identified. These

results are in good agreement with the EDX analysis and demonstrate the high impact of the pH electrode formulation on the CC surface, on the electrode/CC interaction and finally on the performance.

The acidic conditions lead to strong modification of the CC surface which has certainly consequences on both the adhesion of the electrode on CC (SI5) and impedance which were respectively observed lower and higher than for pH7. In the light of XRD analysis it can be supposed that a chlorine based layer weakly attached to the surface favors the electrode delamination whereas a Cu_2O layer on the CC enhances the adhesion of the electrode and indeed is beneficial to the performance (as already observed elsewhere).[22]

4. *Conclusion:*

Electrochemical performance has been compared for the Si-CMC electrodes prepared in different aqueous pH conditions. An enhanced electrochemical behavior was observed for pH=7, confirming literature results.[15] In acidic formulation condition (pH=1 and 3) Si-CMC covalent interaction have been verified by IR and XPS measurements likely associated with both low electrode-CC and high CMC-CMC interactions. For the all studied electrodes the main performance limitation was shown to come from the SEI formation. Although acidic conditions and the formation of covalent Si-CMC bonds are usually suggested to be part of an artificial SEI acting as protective layer to limit the electrolyte degradation [10,13], in this study, the best stability was observed for pH=7. A good Si dispersion is observed in the pH=7 electrode and a non-blocking SEI, though unstable, allowing a good access to the porosity while cycling. Contrarily the pH=3 bring a non-efficient SEI. Moreover acidic condition leads to strong modification of CC, unfavorable to a good adhesion of the electrode to the CC, while a neutral pH leads to a slight oxidation of the CC (Cu_2O) able to prevent electrode delamination.

Acknowledgment :

The SEM measurements were performed by Didier Cot, the EDX measurements by Bertrand Rebiere at IEM (UMR5635). The Zeta potential measurements were realized under the supervision of Anne Aubert from MACS (UMR5253)

This work has benefited from the grant of the National Agency for Research (ANR) under the program "Investments for future" bearing the reference ANR-10-LABX-05-01.

[1] A.M.W. and J.R. Dahn**, Lithium Insertion in Carbons Containing Nanodispersed Silicon, J. Electrochem. Soc. 142 (1995) 326. https://doi.org/10.1149/1.2043994.
[2] X.H. Liu, L. Zhong, S. Huang, S.X. Mao, T. Zhu, J.Y. Huang, Size-dependent fracture of silicon nanoparticles during lithiation, ACS Nano. 6 (2012) 1522–1531. https://doi.org/10.1021/nn204476h.
[3] C. Daniel, J.O. Besenhard, Handbook of Battery Materials: Second Edition, 2011. https://doi.org/10.1002/9783527637188.
[4] Z.L. Xu, X. Liu, Y. Luo, L. Zhou, J.K. Kim, Nanosilicon anodes for high performance rechargeable batteries, Prog. Mater. Sci. 90 (2017) 1–44. https://doi.org/10.1016/j.pmatsci.2017.07.003.
[5] P. Roy, S.K. Srivastava, Nanostructured anode materials for lithium ion batteries, J. Mater. Chem. A. 3 (2015) 2454–2484. https://doi.org/10.1039/c4ta04980b.
[6] J.S. Bridel, T. Azaïs, M. Morcrette, J.M. Tarascon, D. Larcher, Key parameters governing the reversibility of Si/carbon/CMC electrodes for Li-ion batteries, Chem. Mater. 22 (2010) 1229–1241. https://doi.org/10.1021/cm902688w.
[7] D. Mazouzi, Z. Karkar, C.R. Hernandez, P.J. Manero, D. Guyomard, L. Roué, B. Lestriez, Critical roles of binders and formulation at multiscales of silicon-based composite electrodes, J. Power Sources. (2015). https://doi.org/10.1016/j.jpowsour.2015.01.140.
[8] J. Li, R.B. Lewis, J.R. Dahn, Sodium Carboxymethyl Cellulose, Electrochem. Solid-State Lett. 10 (2007) A17. https://doi.org/10.1149/1.2398725.
[9] B. Lestriez, S. Bahri, I. Sandu, L. Roué, D. Guyomard, On the binding mechanism of CMC in Si negative electrodes for Li-ion batteries, 2007. https://doi.org/10.1016/j.elecom.2007.10.001.
[10] N. Delpuech, D. Mazouzi, N. Dupré, P. Moreau, M. Cerbelaud, J.S. Bridel, J.C. Badot, E. De Vito, D. Guyomard, B. Lestriez, B. Humbert, Critical role of silicon nanoparticles surface on lithium cell electrochemical performance analyzed by FTIR, Raman, EELS, XPS, NMR, and BDS spectroscopies, J. Phys. Chem. C. 118 (2014) 17318–17331. https://doi.org/10.1021/jp503949y.
[11] N.S. Hochgatterer, M.R. Schweiger, S. Koller, P.R. Raimann, T. Wöhrle, C. Wurm, M. Winter, Silicon/Graphite Composite Electrodes for High-Capacity Anodes: Influence of Binder Chemistry on Cycling Stability, Electrochem. Solid-State Lett. 11 (2008) A76. https://doi.org/10.1149/1.2888173.
[12] N. Ding, J. Xu, Y. Yao, G. Wegner, I. Lieberwirth, C. Chen, Improvement of cyclability of Si as anode for Li-ion batteries, J. Power Sources. 192 (2009) 644–651. https://doi.org/10.1016/j.jpowsour.2009.03.017.
[13] D. Mazouzi, B. Lestriez, L. Roué, D. Guyomard, Silicon Composite Electrode with High Capacity and Long Cycle Life, Electrochem. Solid-State Lett. 12 (2009) A215. https://doi.org/10.1149/1.3212894.
[14] J.-S. Bridel, T. Azaïs, M. Morcrette, J.-M. Tarascon, D. Larcher, In Situ Observation and Long-Term Reactivity of Si/C/CMC Composites Electrodes for Li-Ion Batteries, J. Electrochem. Soc. 158 (2011) A750. https://doi.org/10.1149/1.3581024.
[15] U.S. Vogl, P.K. Das, A.Z. Weber, M. Winter, R. Kostecki, S.F. Lux, Mechanism of interactions between CMC binder and si single crystal facets, Langmuir. 30 (2014) 10299–10307. https://doi.org/10.1021/la501791q.
[16] C. Real Hernandez, Z. Karkar, D. Guyomard, B. Lestriez, L. Roué, A film maturation process for improving the cycle life of Si-based anodes for Li-ion batteries, Electrochem. Commun. 61 (2015) 102–105. https://doi.org/10.1016/j.elecom.2015.10.014.
[17] C.R. Hernandez, A. Etiemble, T. Douillard, D. Mazouzi, Z. Karkar, E. Maire, D. Guyomard, B. Lestriez, L. Roué, A Facile and Very Effective Method to Enhance the Mechanical Strength and the Cyclability of Si-Based Electrodes for Li-Ion Batteries, Adv. Energy Mater. 1701787 (2017) 1701787. https://doi.org/10.1002/aenm.201701787.
[18] D. Mazouzi, R. Grissa, M. Paris, Z. Karkar, L. Huet, D. Guyomard, L. Roué, T. Devic, B. Lestriez, CMC-citric acid Cu(II) cross-linked binder approach to improve the electrochemical performance of Si-based electrodes, Electrochim. Acta. (2019).

https://doi.org/10.1016/j.electacta.2019.03.026.
[19] D. Mazouzi, B. Lestriez, L. Roué, D. Guyomard, Silicon Composite Electrode with High Capacity and Long Cycle Life, Electrochem. Solid-State Lett. 12 (2009) A215. https://doi.org/10.1149/1.3212894.
[20] T. Chartrel, M. Ndour, V. Bonnet, S. Cavalaglio, L. Aymard, F. Dolhem, L. Monconduit, J.P. Bonnet, Revisiting and improving the preparation of silicon-based electrodes for lithium-ion batteries: ball milling impact on poly(acrylic acid) polymer binders, Mater. Chem. Front. 3 (2019) 881–891. https://doi.org/10.1039/c8qm00660a.
[21] M.D. Harun-or-Rashid, M.D. Saifur Rahaman, S. Enamul Kabir, M.A. Khan, Effect of hydrochloric acid on the properties of biodegradable packaging materials of carboxymethylcellulose/poly(vinyl alcohol) blends, J. Appl. Polym. Sci. 133 (2016) n/a-n/a. https://doi.org/10.1002/app.42870.
[22] D. Mazouzi, R. Grissa, M. Paris, Z. Karkar, L. Huet, D. Guyomard, L. Roué, T. Devic, B. Lestriez, CMC-citric acid Cu(II) cross-linked binder approach to improve the electrochemical performance of Si-based electrodes, Electrochim. Acta. 304 (2019) 495–504. https://doi.org/10.1016/j.electacta.2019.03.026.
[23] Y. Hoshi, Y. Narita, K. Honda, T. Ohtaki, I. Shitanda, M. Itagaki, Optimization of reference electrode position in a three-electrode cell for impedance measurements in lithium-ion rechargeable battery by finite element method, J. Power Sources. 288 (2015) 168–175. https://doi.org/10.1016/j.jpowsour.2015.04.065.
[24] M. Gauthier, D. Mazouzi, D. Reyter, B. Lestriez, P. Moreau, D. Guyomard, L. Roué, A low-cost and high performance ball-milled Si-based negative electrode for high-energy Li-ion batteries, Energy Environ. Sci. 6 (2013) 2145–2155. https://doi.org/10.1039/c3ee41318g.
[25] Z. Karkar, D. Mazouzi, C.R. Hernandez, D. Guyomard, L. Roué, B. Lestriez, Threshold-like dependence of silicon-based electrode performance on active mass loading and nature of carbon conductive additive, Electrochim. Acta. (2016). https://doi.org/10.1016/j.electacta.2016.08.118.
[26] C. Reale Hernandez, A. Etiemble, D. Mazouzi, Z. Karkar, E. Maire, D. Guyomard, B. Lestriez, L. Roué., A Facile and Very Effective Method to Enhance the Mechanical Strength and the Cyclability of Si-Based Electrodes for Li-Ion Batteries. Sous presse, Adv. Energy Mater. 1701787 (2017) 1–13. https://doi.org/10.1002/aenm.201701787.
[27] K. Tasaki, A. Goldberg, J.-J. Lian, M. Walker, A. Timmons, S.J. Harris, Solubility of Lithium Salts Formed on the Lithium-Ion Battery Negative Electrode Surface in Organic Solvents, J. Electrochem. Soc. 156 (2009) A1019–A1027. https://doi.org/10.1149/1.3239850.